Pauli Spin Blockade and the Ultrasmall Magnetic Field Effect

Jeroen Danon,[1] Xuhui Wang,[2] and Aurélien Manchon[2]

[1]*Niels Bohr International Academy, Niels Bohr Institute, University of Copenhagen, Blegdamsvej 17, 2100 Copenhagen, Denmark*
[2]*King Abdullah University of Science and Technology (KAUST), Physical Science and Engineering Division, Thuwal 23955-6900, Saudi Arabia*

(Received 23 March 2013; published 6 August 2013)

Based on the spin-blockade model for organic magnetoresistance, we present an analytic expression for the polaron-bipolaron transition rate, taking into account the effective nuclear fields on the two sites. We reveal the physics behind the qualitatively different magnetoconductance line shapes observed in experiment, as well as the ultrasmall magnetic field effect (USFE). Since our findings agree in detail with recent experiments, they also indirectly provide support for the spin-blockade interpretation of organic magnetoresistance. In addition, we predict the existence of a similar USFE in semiconductor double quantum dots tuned to the spin-blockade regime.

DOI: 10.1103/PhysRevLett.111.066802 PACS numbers: 73.50.−h, 71.38.Mx, 73.43.Qt

The discovery some ten years ago of spin injection in organic semiconductors [1] and a giant magnetoresistance in organic spin valves [2,3] triggered the birth of the thriving field of organic spintronics [4], which offers interesting new physics and the potential of industrial applications. An exciting phenomenon in this field is a large (up to 20%) magnetoresistance observed in different organic materials [5–7], usually at small magnetic fields (1–10 mT) but sometimes at larger fields (10–100 mT) and persisting up to room temperature. Since its discovery in 2004, different explanations for this organic magnetoresistance (OMAR) have been proposed: For bipolar devices, it was suggested that spin-dependent electron-hole recombination and dissociation rates could be responsible [8,9], whereas a model based on nuclear-field-mediated bipolaron formation could explain OMAR in both bipolar and unipolar devices [10–12].

More recently, an organic magnetoresistive effect on an even smaller field scale (0.1–1 mT) has been observed in unipolar as well as bipolar devices [13]. This ultrasmall magnetic field effect (USFE) is manifested by a sign reversal of the magnetoconductance (MC) at very small fields (scaling with the width of the MC curve), which creates two small peaks (dips) around zero field for devices with a negative (positive) MC [13]. An explanation was suggested in terms of enhanced singlet-triplet mixing close to the crossings of the hyperfine sublevels of pairs of charge carriers (polarons) coupled to single nuclear spins [14]. This explanation is still under debate, mainly because it is expected that a single polaron in reality couples to many nuclear spins [15–17]. Others attribute the USFE to the interplay of the polaron Zeeman and exchange splittings [18], which could be relevant for materials with strong coherent intersite coupling.

Here, we study the OMAR line shape as it naturally emerges from the spin-blockade model of Ref. [10]. We present an analytic expression for the charge current through a polaron-bipolaron link for a given realization of the nuclear fields. Our results reproduce the USFE and the different linewidths as observed in experiment and in numerical calculations based on the same semiclassical approach [19], and from our analytic insight we can identify the underlying physical mechanisms. We thus not only reveal the physical origin of the USFE but thereby also provide support for the spin-blockade model capturing the underlying physics of OMAR.

We note that many interesting aspects of spin-blockade physics have already been investigated in the seemingly foreign field of spin qubits hosted in semiconductor quantum dots [20,21], where spin blockade is commonly used as a tool for single-qubit readout [22,23]. Indeed, the physics of the polaron spin-blockade model for OMAR is very similar to that governing the electron transport through a double quantum dot in the spin-blockade regime [21]. Our investigation thus builds on the theoretical framework of Ref. [21], and our explanation of the USFE relies on a subtlety which was not addressed in Ref. [21]. We therefore also provide a refined understanding of quantum dot spin-blockade physics and claim that the USFE also must be present in electron transport through double quantum dots. Indeed, a close inspection of the experimental data presented in Ref. [21] also seems to reveal a faint USFE, which always has been ignored. In fact, due to its tunability, we expect that a double quantum dot might be the best system to experimentally explore the USFE in more detail.

Let us first briefly review the bipolaron model for OMAR presented in Ref. [10]. Electric current flows through the organic material as polarons hop between different localized molecular sites. Typically, the sites participating in transport do not form a regular lattice, and all have a random energy offset with a distribution width σ of 0.1–0.2 eV [10]. Sites with a relatively large negative energy offset are likely to trap a polaron for a long time, but since the on-site polaron-polaron repulsion is typically of the same order of magnitude as σ, such

occupied sites can often still take part in transport by temporarily hosting a pair of polarons, i.e., a bipolaron.

Because of a relatively large orbital level spacing, most energetically accessible bipolaron states are spin singlets. This makes the polaron-bipolaron transition spin selective, ultimately leading to OMAR. The mechanism can be understood from Fig. 1, where we focus on a single polaron-bipolaron transition. We assume that the spins of the two encountering polarons are random, and for simplicity we describe the problem in the basis of spin eigenstates quantized along the direction of the local magnetic fields $\mathbf{B}_{L,R}$. Two possible initial spin states are depicted: (i) the left spin antiparallel and the right spin parallel to the local field and (ii) both spins parallel. In the absence of an external field, the magnetic fields at the two sites are the local random effective nuclear fields [Fig. 1(a)]. Generally, all initial states can then transition to a spin-singlet bipolaron and current runs through the system. If, on the other hand, a magnetic field much larger than the typical nuclear fields is applied, then $\mathbf{B}_L$ and $\mathbf{B}_R$ are (almost) parallel [Fig. 1(b)]. In this case, situation (ii) is a spin triplet, out of which a bipolaron cannot be formed: the current is blocked. Of course, in experiment, there are many possible paths for charge carriers through the material and not all of them contain bipolaron sites. The visibility of all effects of spin blockade will thus be reduced, but the characteristic features survive [10].

In this work, we will focus on the physics of a *single* polaron-bipolaron transition and its MC line shape. To describe the transition, we use five states: the four possible initial spin states of the polaron pair (both sites hosting one polaron)—one spin-singlet state $|S\rangle$ and three spin-triplet states $|T_0\rangle$ and $|T_\pm\rangle$—and the spin-singlet bipolaron state $|S_b\rangle$. The Hamiltonian we use to describe the coherent dynamics of these states reads [21]

$$\hat{H} = \begin{pmatrix} B_s^z & B_s^- & 0 & -B_a^- & 0 \\ B_s^+ & 0 & B_s^- & B_a^z & 0 \\ 0 & B_s^+ & -B_s^z & B_a^+ & 0 \\ -B_a^+ & B_a^z & B_a^- & 0 & t \\ 0 & 0 & 0 & t & -\Delta \end{pmatrix}, \quad (1)$$

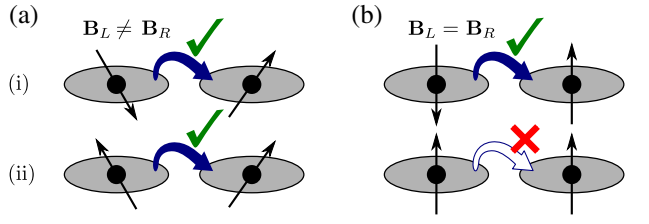

FIG. 1 (color online). When a site already contains a polaron (the right site in the pictures), charge transport through this site relies on the formation of a bipolaron (thick blue arrows). This bipolaron must be a spin singlet, which leads to spin blockade.

written in the basis $\{|T_+\rangle, |T_0\rangle, |T_-\rangle, |S\rangle, |S_b\rangle\}$. This Hamiltonian includes a coupling energy t between the two singlets (which enables polaron hopping) and the relative energy offset (detuning) Δ of the bipolaron state, typically $\Delta \sim \sigma$. The effect of the local magnetic fields $\mathbf{B}_{L,R}$ is expressed in terms of the sum and difference fields $\mathbf{B}_s = (1/2)(\mathbf{B}_L + \mathbf{B}_R)$ and $\mathbf{B}_a = (1/2)(\mathbf{B}_L - \mathbf{B}_R)$, and we use the notation $B^{\pm}_{s(a)} = (1/\sqrt{2})(B^x_{s(a)} \pm iB^y_{s(a)})$. Note that we have set $g\mu_B = 1$ for convenience.

As pointed out in Ref. [21], we can deduce already from Eq. (1) that there exist in the space of $(\mathbf{B}_L, \mathbf{B}_R)$ so-called "stopping points" where the current is blocked. To see this, we take the spin quantization axis to point along $\mathbf{B}_s$, which amounts to setting $B_s^{\pm} \to 0$ in Eq. (1). Then, we find that current vanishes when $\mathbf{B}_a \parallel \mathbf{B}_s$ or $\mathbf{B}_a \perp \mathbf{B}_s$, since at these points one or more of the triplet states are not coupled to $|S\rangle$. The sum and difference fields $\mathbf{B}_{s,a}$ both contain a contribution from the effective nuclear fields $\mathbf{K}_{L,R}$ on the two sites, whereas the external field $\mathbf{B}_{\text{ext}}$ only adds to the sum field: $\mathbf{B}_s = \mathbf{K}_s + B_{\text{ext}}\hat{z}$ and $\mathbf{B}_a = \mathbf{K}_a$. For a given random realization of $\mathbf{K}_{L,R}$, one can thus always find a field B_{ext} for which $\mathbf{B}_a \perp \mathbf{B}_s$, and a sweep of B_{ext} for a *fixed* $\mathbf{K}_{L,R}$ will always exhibit a stopping point where the current vanishes. The position of this stopping point is determined by the relative orientations of $\mathbf{K}_s$ and $\mathbf{K}_a$ and is thus random. In an experiment, one usually sweeps B_{ext} so slowly that at each measurement, many configurations of the fields $\mathbf{K}_{L,R}$ are probed. As a result, the stopping points are averaged out and one finds a smooth MC curve [21].

However, this is not the full story. A subtlety, not discussed in Ref. [21], is that there exists one more stopping point [24]: When $\mathbf{B}_s = 0$, the triplet subspace in the Hamiltonian is degenerate and Eq. (1) can be equivalently written in terms of one coupled triplet state

$$|T_m\rangle = \frac{-B_a^-|T_+\rangle + B_a^z|T_0\rangle + B_a^+|T_-\rangle}{|\mathbf{B}_a|}$$

and two orthogonal triplet states $|T_1\rangle$ and $|T_2\rangle$ which have $\langle T_{1,2}|\hat{H}|S\rangle = 0$ and are thus blocked. Why would we bother? We argued above that stopping points occur at random positions, leaving no trace after averaging over $\mathbf{K}_{L,R}$. This new stopping point, however, is fundamentally different from the ones discussed above: It suppresses current close to where $\mathbf{B}_{\text{ext}} = -\mathbf{K}_s$, which is *always* in the vicinity of $B_{\text{ext}} = 0$. It is therefore possible that after averaging over $\mathbf{K}_{L,R}$, this new stopping point leaves a trace in the MC curve: a small dip around zero field, like the USFE.

Let us now explicitly calculate the current as governed by this polaron-bipolaron transition. To describe charge transport, we write a time-evolution equation for the 5×5 density matrix of the system. To the coherent evolution dictated by $\hat{H}$, we add incoherent rates describing dissociation of the bipolaron to the environment and hopping of a new polaron onto the empty left site. This yields (where we have set $\hbar$ to 1)

$$\frac{\partial\hat{\rho}}{\partial t} = -i[\hat{H},\hat{\rho}] - \frac{\Gamma}{2}\{\hat{P}_b,\hat{\rho}\} + \frac{\Gamma}{4}\rho_{b,b}(1-\hat{P}_b)\hat{\mathbb{1}}, \quad (2)$$

where Γ is the rate of bipolaron dissociation to the environment, $\hat{P}_b = |S_b\rangle\langle S_b|$ is the projection operator onto the bipolaron state, and $\hat{\mathbb{1}}$ is the identity matrix. In writing so, we assumed for simplicity that the refilling of the left site takes place immediately after the dissociation of the bipolaron. If this is not the case, the prefactor for the current changes but the MC characteristics stay the same.

We add the normalization condition $\mathrm{Tr}[\hat{\rho}] = 1$ to the set of equations and then solve $\partial_t\hat{\rho}^{(\mathrm{eq})} = 0$ to find the stationary density matrix. The charge current is then given by $I = e\Gamma\rho_{b,b}^{(\mathrm{eq})}$ and can be found explicitly. We assume for convenience that $\Gamma \gg t$, B_s, B_a, Δ is the largest energy scale in the problem [12], and then find

$$I = e\Gamma_s\frac{4x^2\sin^2\phi}{x^4+ax^2+1}, \quad (3)$$

in terms of $x \equiv B_s/B_a$. Here, $\Gamma_s \equiv t^2/\Gamma$ is the singlet-singlet hopping rate from the left to the right site and ϕ is the angle between $\mathbf{B}_s$ and $\mathbf{B}_a$ [25]. We also used

$$a = \frac{\Gamma_s^2}{B_a^2}\left(3+\frac{1}{\cos^2\phi}\right) - 2\cos 2\phi. \quad (4)$$

We see that all stopping points predicted above are indeed reflected in Eq. (3): At $B_s = 0$, we have $x = 0$, which yields $I = 0$, and $\mathbf{B}_a \parallel \mathbf{B}_s$ or $\mathbf{B}_a \perp \mathbf{B}_s$ corresponds to $\phi = 0$, π or $\phi = \pi/2$, respectively, both also giving $I = 0$.

Equation (3) is the most important analytic result of our work. It gives the current for one single realization of $\mathbf{K}_L$, $\mathbf{K}_R$, and B_{ext}. The MC measured in experiment is found by averaging Eq. (3) over the random nuclear fields. In contrast to the analytic results presented in Ref. [21], our result is valid for arbitrary Γ_s and not only for limiting cases. One word of caution is required here concerning the interpretation of Eq. (3): If one wants to plot $I(B_{\mathrm{ext}})$ for a single realization of $\mathbf{K}_{L,R}$, one should not only use $B_s = |\mathbf{K}_s + B_{\mathrm{ext}}\hat{z}|$ in Eq. (3) but also implement the dependence of ϕ on B_{ext} implied by $\cos\phi = (\mathbf{B}_s\cdot\mathbf{B}_a)/B_sB_a$.

Let us now investigate Eq. (3) and see what we can infer about the line shape of the predicted MC curve. We always have $a > -2$, which ensures that $I \geq 0$ everywhere. The current vanishes for $x = 0$ or $x \to \infty$, and in the range $x \in [0,\infty]$, we have a single maximum at $x = 1$ where the current is $I_{\max} = 4e\Gamma_s\sin^2\phi/(a+2)$. In Fig. 2(a), we plot the expression given in Eq. (3) for different a. The FWHMs w_- of the dip around $x = 0$ and w_+ of the overall peak structure (as indicated in the plot for $a = 4$) are found to be $w_\pm^2 = 2 + (1/2)a \pm \sqrt{3+2a+(1/4)a^2}$.

We see from Eq. (4) that an important parameter is Γ_s/K, the ratio of the intersite hopping rate and the typical magnitude of the nuclear fields K, typically ~ 0.1 μeV [15]. We will thus now investigate the cases of small and large Γ_s/K.

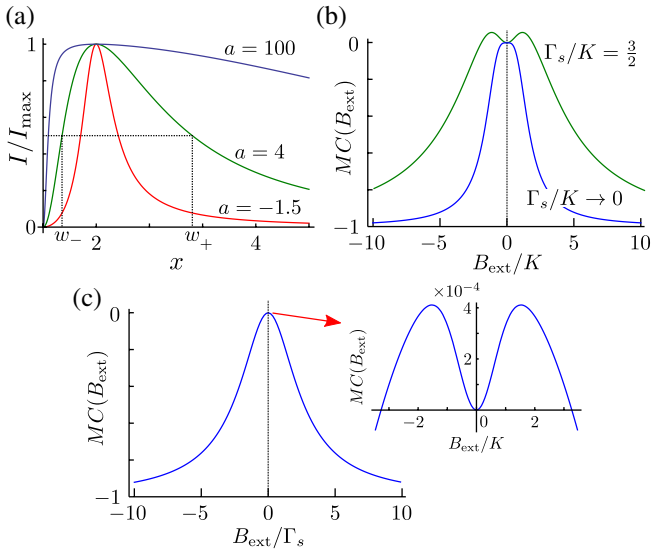

FIG. 2 (color online). (a) The current given by Eq. (3) as a function of $x = B_s/B_a$ for fixed B_a and ϕ, evaluated for different parameters a. (b),(c) The averaged MC. (b) The blue trace represents $\Gamma_s/K \ll 1$. The field B_{ext} is plotted in units of $K = \langle K_{L,R}^2\rangle^{1/2}$. The peak of this curve is flat [21]. The green trace represents $\Gamma_s/K = 3/2$. (c) $\Gamma_s/K = 50$. Now, B_{ext} is plotted in units of Γ_s. Inset: The range where $B_{\mathrm{ext}} \sim K$.

In the limit of $\Gamma_s/K \ll 1$, we can write

$$I \approx e\Gamma_s\frac{4x^2\sin^2\phi}{x^4-2x^2\cos 2\phi+1} = \Gamma_s(\mathbf{n}_L\times\mathbf{n}_R)^2, \quad (5)$$

where we used the unit vectors $\mathbf{n}_{L,R} = \mathbf{B}_{L,R}/B_{L,R}$. As it should, this result coincides with that of Ref. [21] in the same limit: There are no intersite exchange effects, and the situation is exactly like the picture of Fig. 1 where the current only depends on the relative orientations of $\mathbf{B}_L$ and $\mathbf{B}_R$. As was shown in Ref. [21], Eq. (5) can be averaged analytically over random $\mathbf{K}_{L,R}$ taken from a normal distribution, yielding a MC curve with a flat peak at $B_{\mathrm{ext}} = 0$, a maximum of $\langle I\rangle_{\max} \sim e\Gamma_s$, and a linewidth of $\sim K$. Indeed, for all $a \in [-2,2]$, we find that $w_+ \sim 1$, so for any ϕ the current is suppressed when $x \gtrsim 1$. In Fig. 2(b) (blue trace), we plot the resulting MC line shape, where we defined $\mathrm{MC}(B_{\mathrm{ext}}) = [I(B_{\mathrm{ext}}) - I(0)]/I(0)$.

In the opposite limit of $\Gamma_s/K \gg 1$, we have $a \approx (\Gamma_s/B_a)^2(3+\cos^{-2}\phi) \gg 1$. We can already see from the properties of Eq. (3) that in this case, $\langle I\rangle_{\max} \sim eK^2/\Gamma_s$, and that $w_+ \approx a^{1/2} \sim \Gamma_s/K$ implies a MC linewidth of $\sim\Gamma_s$. Indeed, Γ_s sets the level broadening of $|S\rangle$, and as long as $B_s \lesssim \Gamma_s$, generally all three triplet states can efficiently transition to $|S\rangle$ with the coupling provided by $\mathbf{B}_a$. The width of the dip around the stopping point at $x = 0$ is $w_- \approx a^{-1/2} \sim K/\Gamma_s$ in terms of x, or $\sim K^2/\Gamma_s$ in terms of B_s. This energy scale can also be understood: If $B_s = 0$, the decay rate of $|T_m\rangle$ is $\Gamma_t \sim K^2/\Gamma_s$, which is the only energy relevant in the triplet subspace. When $B_s \gtrsim \Gamma_t$, the

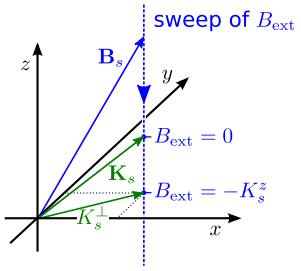

FIG. 3 (color online). When $B_{\rm ext}$ is swept for a given realization of $\mathbf{K}_{L,R}$, the field $\mathbf{B}_s$ (blue arrow) follows a trace like the dashed blue line. We indicated with green arrows $\mathbf{K}_s$ as well as $K_s^\perp$, which equals the minimum value of B_s.

decay of the other two triplet states becomes comparable to Γ_t and the blockade is lifted.

In this limit of large Γ_s/K, the current cannot be averaged analytically over the nuclear fields, and one has to evaluate the integrals over the distribution of $\mathbf{K}_{L,R}$ numerically. Figure 2(c) shows a plot of the MC integrated over normal distributions for all six components of $\mathbf{K}_L$ and $\mathbf{K}_R$. For all components, we used a standard deviation of $K/\sqrt{3}$ and we have set $\Gamma_s/K = 50$. The resulting line shape is Lorentzian since it is determined by the level broadening of $|S\rangle$. Close to zero field, where $B_{\rm ext} \sim K$, we find a very faint USFE, as shown in the inset. When we set Γ_s/K even larger, we find that the visibility of this USFE is suppressed further, ultimately reaching zero.

We can understand this USFE from the expression for the current given in Eq. (3). For a given realization of $\mathbf{K}_{L,R}$, the current trace $I(B_{\rm ext})$ "misses" the zero-field stopping point by $K_s^\perp = \sqrt{(K_s^x)^2 + (K_s^y)^2}$, as illustrated in Fig. 3. Some realizations have $K_s^\perp \geq B_a$ so that the current trace has a single maximum [see Fig. 2(a)]. Other realizations have $K_s^\perp < B_a$, and the current exhibits a dip at small fields, the position of the dip at $B_{\rm ext} = -K_s^z$. For large Γ_s/K, the dip around the zero-field stopping point becomes narrow, of the order of $\sim K^2/\Gamma_s \ll K$, and only the very few curves of $I(B_{\rm ext})$ with $K_s^\perp \lesssim K^2/\Gamma_s$ have an appreciable dip. This can still produce a faint dip in the averaged current. However, the position of each single-realization narrow dip is at $B_{\rm ext} = -K_s^z$, so averaging over K_s^z makes the averaged dip even less pronounced and results in a dip width of $\sim K$.

The regime to look for a pronounced USFE is thus at intermediate $\Gamma_s/K \sim 1$. In Fig. 2(b) (green trace), we plot the averaged MC for $\Gamma_s/K = 3/2$ and we see indeed a strong USFE, its visibility being $\sim 5\%$. This regime is optimal for the USFE since here the width of the zero-field dip is still $\sim K$, but the symmetric situation where the current only depends on the angle between $\mathbf{n}_L$ and $\mathbf{n}_R$ is significantly perturbed. In other words, at $\Gamma_s/K \to 0$, the overall MC linewidth is minimal and $\sim K$. The two USFE "bumps" are still there but are split by the same energy scale $\sim K$ and thus appear just left and right of the top of the MC curve. In the limit of $\Gamma_s/K = 0$, the bumps and the underlying MC curve have exactly compatibly shaped line shapes, together resulting in the characteristic flat peak. If one moves away from $\Gamma_s/K = 0$, the underlying MC line shape becomes broader, which makes the USFE bumps more visible. However, as soon as Γ_s/K becomes too large, one enters the regime discussed above, where the USFE disappears again. The optimal regime is thus at $\Gamma_s/K \sim 1$, in agreement with the results presented in Figs. 2(b) and 2(c) as well as with previously obtained numerical results [12].

To summarize, we studied the two-site spin-blockade model for OMAR and derived an analytic expression for the polaron-bipolaron transition rate, which provides an explanation of the USFE in terms of a persistent spin blockade at the special point where the average effective field vanishes $B_s = 0$. Our work also deepens the understanding of spin-blockade physics in semiconductor quantum dots, and we predict the existence of an USFE in these systems as well.

We acknowledge helpful feedback from M. S. Rudner and P. A. Bobbert.

[1] V. Dediu, M. Murgia, F. Matacotta, C. Taliani, and S. Barbanera, Solid State Commun. **122**, 181 (2002).
[2] J. Kalinowski, M. Cocchi, D. Virgili, P. Di Marco, and V. Fattori, Chem. Phys. Lett. **380**, 710 (2003).
[3] Z. H. Xiong, D. Wu, Z. V. Vardeny, and J. Shi, Nature (London) **427**, 821 (2004).
[4] V. A. Dediu, L. E. Hueso, I. Bergenti, and C. Taliani, Nat. Mater. **8**, 707 (2009).
[5] T. L. Francis, Ö. Mermer, G. Veeraraghavan, and M. Wohlgenannt, New J. Phys. **6**, 185 (2004).
[6] Ö. Mermer, G. Veeraraghavan, T. L. Francis, Y. Sheng, D. T. Nguyen, M. Wohlgenannt, A. Köhler, M. K. Al-Suti, and M. S. Khan, Phys. Rev. B **72**, 205202 (2005).
[7] F. L. Bloom, W. Wagemans, M. Kemerink, and B. Koopmans, Phys. Rev. Lett. **99**, 257201 (2007).
[8] V. Prigodin, J. Bergeson, D. Lincoln, and A. Epstein, Synth. Met. **156**, 757 (2006).
[9] P. Desai, P. Shakya, T. Kreouzis, and W. P. Gillin, Phys. Rev. B **76**, 235202 (2007).
[10] P. A. Bobbert, T. D. Nguyen, F. W. A. van Oost, B. Koopmans, and M. Wohlgenannt, Phys. Rev. Lett. **99**, 216801 (2007).
[11] W. Wagemans, F. L. Bloom, P. A. Bobbert, M. Wohlgenannt, and B. Koopmans, J. Appl. Phys. **103**, 07F303 (2008).
[12] A. J. Schellekens, W. Wagemans, S. P. Kersten, P. A. Bobbert, and B. Koopmans, Phys. Rev. B **84**, 075204 (2011).
[13] T. D. Nguyen, B. R. Gautam, E. Ehrenfreund, and Z. V. Vardeny, Phys. Rev. Lett. **105**, 166804 (2010).
[14] T. D. Nguyen, G. Hukic-Markosian, F. Wang, L. Wojcik, X.-G. Li, E. Ehrenfreund, and Z. V. Vardeny, Nat. Mater. **9**, 345 (2010).
[15] D. R. McCamey, K. J. van Schooten, W. J. Baker, S.-Y. Lee, S.-Y. Paik, J. M. Lupton, and C. Boehme, Phys. Rev. Lett. **104**, 017601 (2010).

[16] P. A. Bobbert, Nat. Mater. **9**, 288 (2010).
[17] K. Schulten and P. G. Wolynes, J. Chem. Phys. **68**, 3292 (1978).
[18] N. J. Harmon and M. E. Flatté, Phys. Rev. B **85**, 245213 (2012).
[19] S. P. Kersten, A. J. Schellekens, B. Koopmans, and P. A. Bobbert, Phys. Rev. Lett. **106**, 197402 (2011).
[20] K. Ono, D. G. Austing, Y. Tokura, and S. Tarucha, Science **297**, 1313 (2002).
[21] O. N. Jouravlev and Y. V. Nazarov, Phys. Rev. Lett. **96**, 176804 (2006).
[22] F. H. L. Koppens, C. Buizert, K. J. Tielrooij, I. T. Vink, K. C. Nowack, T. Meunier, L. P. Kouwenhoven, and L. M. K. Vandersypen, Nature (London) **442**, 766 (2006).
[23] D. J. Reilly, J. M. Taylor, J. R. Petta, C. M. Marcus, M. P. Hanson, and A. C. Gossard, Science **321**, 817 (2008).
[24] One could argue that $\mathbf{B}_a = 0$ is also a stopping point, but it is not of any interest since it occurs independently from B_{ext} and therefore leaves no traces in the MC curve. In that sense, it is also not really a stopping *point*. Besides, it is captured by the model in Ref. [21] since it is equivalent to having $\mathbf{B}_a \parallel \mathbf{B}_s$ *and* $\mathbf{B}_a \perp \mathbf{B}_s$.
[25] If one would relax the assumption $\Gamma \gg \Delta$, one finds the same expression but with $\Gamma_s \to t^2/\sqrt{\Gamma^2 + 4\Delta^2}$ and an extra prefactor $\Gamma/\sqrt{\Gamma^2 + 4\Delta^2}$. A finite detuning Δ thus merely leads to a suppression of the current as well as a smaller effective hopping rate.